Effect of Treatment Media on the Agglomeration of Titanium Dioxide Nanoparticles: Impact on Genotoxicity, Cellular Interaction, and Cell Cycle

Raju Y. Prasad,[†] Kathleen Wallace,[‡] Kaitlin M. Daniel,[†] Alan H. Tennant,[‡] Robert M. Zucker,[§] Jenna Strickland,[†] Kevin Dreher,[⊥] Andrew D. Kligerman,[‡] Carl F. Blackman,[‡] and David M. DeMarini[‡,*]

[†]Student Services Contractor, [‡]Integrated Systems Toxicology Division, [§]Toxicology Assessment Division, and [⊥]Environmental Public Health Division, U.S. Environmental Protection Agency, Research Triangle Park, North Carolina 27711, United States

ABSTRACT The widespread use of titanium dioxide (TiO_2) nanoparticles in consumer products increases the probability of exposure to humans and the environment. Although TiO_2 nanoparticles have been shown to induce DNA damage (comet assay) and chromosome damage (micronucleus assay, MN) *in vitro*, no study has systematically assessed the influence of medium composition on the physicochemical characteristics and genotoxicity of TiO_2 nanoparticles. We assessed TiO_2 nanoparticle agglomeration, cellular interaction, induction of genotoxicity, and influence on cell cycle in human lung epithelial cells using three different nanoparticle-treatment media: keratinocyte growth medium (KGM) plus 0.1% bovine serum albumin (KB); a synthetic broncheoalveolar lavage fluid containing PBS, 0.6% bovine serum albumin and 0.001% surfactant (DM); or KGM with 10% fetal bovine serum (KF). The comet assay showed that TiO_2 nanoparticles induced similar amounts of DNA damage in all three media, independent of the amount of agglomeration, cellular interaction, or cell-cycle changes measured by flow cytometry. In contrast, TiO_2 nanoparticles induced MN only in KF, which is the medium that facilitated the lowest amount of agglomeration, the greatest amount of nanoparticle cellular interaction, and the highest population of cells accumulating in S phase. These results with TiO_2 nanoparticles in KF demonstrate an association between medium composition, particle uptake, and nanoparticle interaction with cells, leading to chromosomal damage as measured by the MN assay.

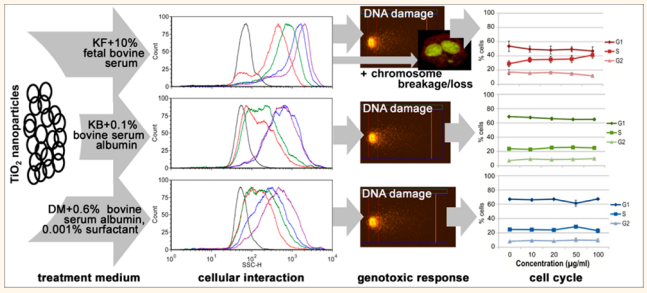

KEYWORDS: titanium dioxide nanoparticles · genotoxicity · micronuclei · comet assay · DNA damage · flow cytometry · cell cycle · dark-field microscopy · electron microscopy

The number of consumer and commercial products containing nanoparticles already exceeds 800 and is growing at an exponential rate.[1] Metal oxide nanoparticles, in particular, are currently present in the environment due to industrial processes and consumer products available on the market.[2] This increased usage requires an improved understanding of the potential risks and hazards associated with human exposure. Specifically, it is critically important to identify those physicochemical characteristics of nanoparticles that may cause detrimental health effects.

Titanium dioxide (TiO_2) nanoparticles, which are one of the most widely used engineered nanoparticles, are used in sunscreens and cosmetics because of their absorptive properties and have also been used as a wastewater disinfectant due to their photocatalytic properties.[1] The National Institute for Occupational Safety and Health has made efforts to determine two different size/concentration levels for worker safety due to the potential for nanosized TiO_2 particles to cause toxicity.[2] Furthermore, the crystal structure of TiO_2 nanoparticles has been shown previously to play a role in the toxicity of such nanoparticles, with the anatase isoform inducing greater inflammation than the rutile isoform *in vivo*.[3]

Several studies over the past decade have used the single cell gel electrophoresis (comet) assay and cytokinesis-blocked micronucleus (MN) assay to investigate the

* Address correspondence to demarini.david@epa.gov.

Received for review May 23, 2012 and accepted February 6, 2013.

Published online February 06, 2013
10.1021/nn302280n

in vitro genotoxicity of TiO_2 nanoparticles. In some studies, TiO_2 nanoparticles showed no significant induction of DNA damage based on the comet assay in human peripheral blood lymphocytes[4] or BEAS-2B/IMR-90 cells.[5] However, other studies found that TiO_2 nanoparticles induced DNA damage in BEAS-2B,[6,7] GFSk-S1 cells,[8] and peripheral blood lymphocytes.[9] On the basis of the results with the MN assay, researchers have found that TiO_2 nanoparticles induce chromosomal damage in BEAS-2B cells at 24 h;[7] in SHE fibroblasts at 12, 24, 48, 66, and 72 h;[10] in WIL2-NS cells at 6, 24, and 48 h;[11] and in peripheral blood lymphocytes *in vitro* at 12, 24, and, 48 h.[9] However, another study in BEAS-2B cells showed a significant increase in MN only after a 72 h exposure but not after a 24 or 48 h exposure.[6]

A potential explanation for this discrepancy is in the preparation of the nanoparticles as well as the type of medium in which the cells are cultured and/or treated. Nanoparticle−protein interactions (referred to as the "protein corona" or the association of proteins in a biological medium with the surface of the nanoparticle) have been hypothesized to play an important role in the uptake, distribution, and toxicity of nanoparticles in biological systems; however, it is still unclear how this occurs.[12−16] For example, reactive oxygen species (ROS) produced by exposure to carbon black particles in a Monomac-6 cell line were increased when medium containing 1% bovine serum albumin (BSA) and/or 0.025% surfactant was used.[17] A surfactant (Pluronic F127) used to disperse single-walled carbon nanotubes, and amorphous silica resulted in a lower toxicity in RAW 264.7, a macrophage-like cell line.[13] Gold nanorods induced less toxicity in HeLa cells when serum was used in the cell culture medium, and this was associated with reduced cellular uptake.[18] On the other hand, silica suspended in bronchoalveolar lavage (BAL) fluid showed no differences in the induction of pulmonary inflammation and lactate dehydrogenase in A549 (a human lung cell line) compared to a phosphate buffer solution.[19]

Despite the apparent role of medium composition and other factors on the genotoxicity of TiO_2 nanoparticles, no systematic assessment of these parameters has been performed.[20−23] Consequently, there is no consensus or harmonized guidance on how to prepare nanoparticles for *in vitro* toxicity testing or to formulate the composition of the medium. Additionally, there is no consensus on what physicochemical characteristics of the particles should be determined and reported or for the physicochemical characteristics that may influence genotoxicity.[22] Some genotoxicity studies have not characterized the nanoparticles in dispersion;[7] nonetheless, physical characteristics such as surface area, primary particle size, and agglomeration/stability of the dispersion are thought to play a role in the toxicity of nanoparticles.[24−27]

The relationship between the protein corona and its role in genotoxicity is not fully understood.[22] Cationic polysaccharide nanoparticles (60 nm) dispersed in serum, no serum, or BSA were shown to have differences in cellular uptake, DNA damage, and MN frequencies in 16HBE14o- human bronchial epithelial cells.[28] Corradi *et al.*[29] studied an array of nanoparticles (Lys-SiO_2, TiO_2, ZnO, and multiwalled carbon nanotubes) in the presence or absence of 10% serum in A549 cells after a 4 h exposure and showed increases in MN frequency in cells treated with ZnO in the presence of serum. Thus, there is a need to determine the most appropriate procedures by which to characterize TiO_2 nanoparticles, to measure their uptake into cells, and to evaluate their genotoxicity in order to produce data useful for assessing the safety of nanoparticles.[30,31]

To address this issue, we have determined the cytotoxicity and genotoxicity of 10−100 μg/mL of TiO_2 nanoparticles in human lung epithelial cells (BEAS-2B) exposed in three different media that have been used previously in nanotoxicology studies.[13,17−19] We chose this concentration range to be consistent with previously published literature on the *in vitro* genotoxicity of TiO_2 nanoparticles.[4−11] We diluted and sonicated TiO_2 nanoparticles in either (a) keratinocyte growth medium (KGM) with 0.1% BSA, referred to as KB, (b) a medium that mimics BAL by containing phosphate-buffered saline (PBS) with 0.6% BSA and 0.001% DSPC (1,2-dipalmitoyl-*sn*-glycero-3-phosphocholine, a surfactant) as a biologically relevant medium that can also improve dispersion[17,19] and referred to herein as dispersion medium (DM), or (c) KGM with 10% fetal bovine serum (FBS) and referred to as KF. These media compositions are those of the nanoparticle-treatment media. The cell-treatment media had lower levels of protein compared to the nanoparticle-treatment media, which were composed as follows: KB was KGM + 0.01% BSA, DM was KGM alone, and KF was KGM + 1% FBS. We characterized primary particle size, surface area, purity, and crystal structure by transmission electron microscopy (TEM) and visualized TiO_2 nanoparticles in each treatment medium with scanning electron microscopy (SEM). We also assessed whether proteins in each treatment medium were adsorbed to the nanoparticle surface using sodium dodecyl sulfate-polyacrylamide gel electrophoresis (SDS-PAGE). Lastly, we determined the hydrodynamic diameter/size, polydispersion index (PdI), and zeta-potential by dynamic light scattering (DLS), as well as cellular interaction and cell-cycle effects by flow cytometry.[32,33]

RESULTS AND DISCUSSION

We evaluated the cytotoxicity, genotoxicity, agglomeration, cellular interaction, and effects on cell cycle of TiO_2 nanoparticles prepared in three media: (a) KB, which had a low concentration of protein (0.1% BSA); (b) DM, which had a lower level of protein (0.6% BSA) plus 0.001% surfactant; and (c) KF, which contained 10% FBS. By measuring various physicochemical characteristics, we

have attempted to determine which media influenced the genotoxicity of TiO_2 nanoparticles based on two standard *in vitro* assays: the comet and the MN assays.

Physicochemical Characterization of TiO_2 Nanoparticles in Dry Form and Treatment Medium. Determining the physical characteristics of nanoparticles in dry form and in treatment medium has become important in comparing studies across the literature.[21,23,34] The physical characteristics of Degussa P25 AEROXIDE TiO_2 in dry form were measured by TEM at the University of Kentucky. A representative image is shown in Supplemental Figure 1, and the results are presented in Table 1. The primary particle size was measured to be ~27.5 nm, with a surface area of 49 m^2/g, and the particles were a mixture of anatase and rutile crystal structures. As illustrated by SEM in Figure 1, TiO_2 nanoparticles were qualitatively different in all three treatment media. The KF medium resulted in smaller agglomerated nanoparticles compared to those observed in the other two media.

DLS was used to measure hydrodynamic diameter, PdI, and zeta-potential of nanoparticles in suspension. We initially measured each treatment medium alone and determined that the protein concentrations did not confound the DLS results (Supplemental Figure 2). DLS measurements of TiO_2 nanoparticles in the three treatment media showed that KB resulted in the largest agglomerates, followed by DM and then KF (Figure 2A). After 24 h at 37 °C, the suspension in KB showed larger agglomerates with increasing concentration from the 0 h size measurements, whereas KF did not. DM showed slightly elevated agglomerates at 24 h, with a significant increase compared with KF. Agglomerates in KB were still significantly greater than DM and KF after 24 h (Figure 2B).

Collectively, the results above demonstrate the increasing stability of dispersions with increasing amounts of protein as evidenced by the maintenance of agglomerate size during a 24 h treatment period at concentrations from 10 to 100 μg/mL. The rank order of agglomeration size in treatment media based on the DLS data at 0 and 24 h was KB > DM > KF. Representative graphs of dynamic light scattering data show that TiO_2 agglomeration increased with increasing concentration in each medium (Supplemental Figures 3−5). The hydrodynamic diameter of TiO_2 nanoparticles suspended in distilled water ranged from 273 to 309 nm, consistent with previous studies (Table 2).[26]

We also calculated the PdI, which is a measure of the variance in size measurements, for each concentration in each treatment medium (Table 2). The values for all concentrations in all treatment media were between 0.2 and 0.8, with KB yielding the highest PdI values and KF yielding the lowest. Zeta-potential, a measure of electrokinetic potential that indicates the degree of repulsion between particles, was −0.53 to −8.47 mV for all concentrations in all treatment media at 37 °C (Table 2). To be considered a disperse suspension, these zeta-potential values should be above/below ±30 mV.[35] Thus, our results with both

TABLE 1. Physical Characteristics of TiO_2 Nanoparticles[a]

characteristic	result
primary particle size	27.5 nm[b]
size range	14.2−64.6 nm[b]
surface area	49 m^2/g[b]
% purity	95.1%[b]
crystal form	86% anatase/14% rutile[b]
elemental analysis	Ti = 59.95%[c]

[a] Data from the University of Kentucky (see Materials and Methods).[41,59] [b] Size, surface area, purity, and crystal form of P25 TiO_2 received from the manufacturer were measured independently. Approximately, 150 dry particles were examined by TEM. [c] Elemental analysis by ICP/MS. Because the sample showed high purity, a set of 31 elements was checked to find contaminants. The levels of contaminants in the highest concentration were as follows: Co (971 and 1002 ppm), K (350 and <0.05 ppm), SiO_2 (1578 and 1219 ppm), and V (303 and 315 ppm).

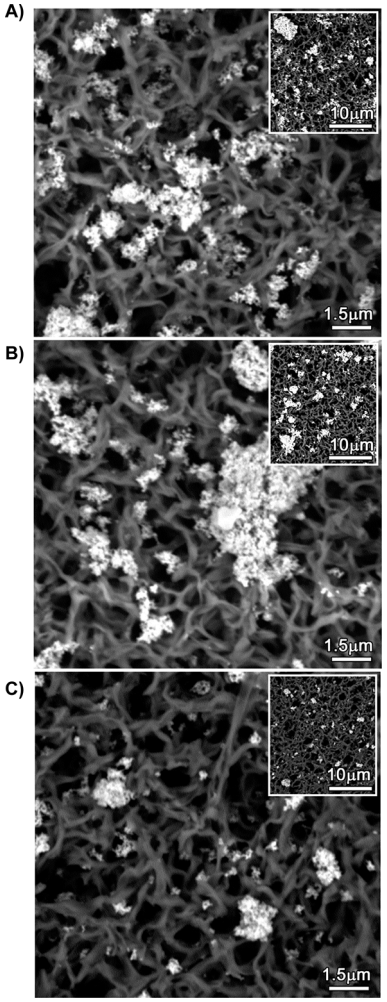

Figure 1. Representative SEM images of TiO_2 nanoparticles dispersed in (A) KB medium, (B) DM medium, and (C) KF medium at 200 μg/mL. Magnification: ~18 000× (large image) and ~3000× (smaller image); the large figures are a 6× magnification of the small (inset) figures. These images show that the nanoparticles form fewer and smaller agglomerates in KF medium (C) than in the other two media (A,B).

PdI and zeta-potential indicate that the nanoparticle "dispersions" were unstable, aggregating and separating out of the liquid phase during the genotoxicity experiments, which is common for medium suspensions of TiO_2 nanoparticles.[26] Zeta-potential of TiO_2 nanoparticles in distilled water was lower than in medium, with a range of −8.7 to −17.2 mV (indicating a more disperse suspension), which has been shown previously (Table 2).[26,36]

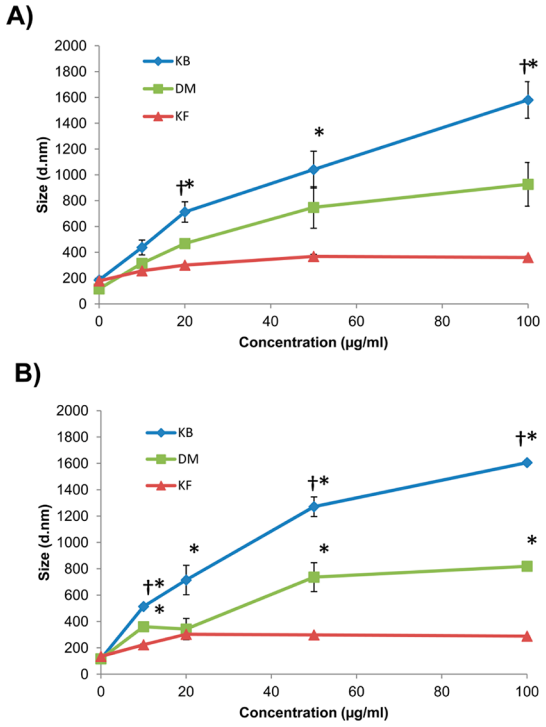

Figure 2. Characterization of TiO_2 nanoparticles in treatment media by dynamic light scattering. Mean hydrodynamic diameter (*d*, nm) was determined for all three treatment media from 0 to 100 μg/mL at (A) t = 0 h and (B) t = 24 h. Data are represented as mean ± SD of three independent measurements; *$p < 0.05$ denotes a significant increase from KF treatment; †$p < 0.05$ denotes a significant increase from DM treatment.

The size, PdI, and zeta-potential of nanoparticles in solution can be influenced by characteristics of the medium such as protein concentration, pH, and type of nanoparticle.[26] In our study, we confirmed this by showing an inverse correlation between protein concentration and average hydrodynamic diameter of TiO_2 agglomerates in medium with the same temperature and pH and similar zeta-potentials. Additionally, we have shown that the protein corona on the nanoparticle surface as determined by SDS-PAGE is associated with the amount of protein in the treatment medium (Supplemental Figure 6). These data indicate that the protein in the medium can adsorb to the nanoparticle surface and play an important role in surface presentation and agglomeration.[16] The ability of metal oxide nanoparticles to adsorb proteins onto their surface has been studied previously;[36,37] however, the biological effects of this are not well-understood.

Determination of Cellular Interaction. TiO_2 nanoparticles can enter cells, resulting in a change in the cytoplasm that can be measured by flow cytometry using side scatter.[32,33,38] Thus, we assessed cellular interaction quantitatively and qualitatively by flow cytometry using a method developed in our laboratory.[32,33] Figure 3A shows a representative side-scatter distribution for concentrations of 10−100 μg/mL of TiO_2 nanoparticles in cells in each treatment medium. Side scatter is thought to indicate the cell granularity and mass of the cells.[39,40] After treatment of the cells with TiO_2 nanoparticles, there are increases in the side scatter (90° direction) of the cells. These values can be quantified using a ratio that compares the histogram of the treated population of cells to an untreated control (Figure 3B). There is a direct relationship between concentration of nanoparticles

TABLE 2. TiO_2 Nanoparticle Characterization in Three Treatment Media and H_2O Measured by Dynamic Light Scattering[a]

medium	concentration (μg/mL)	size (nm)	size after 24 h at 37 °C (nm)	PdI	PdI after 24 h at 37 °C	zeta-potential (mV)
KB	10	437.7 ± 115.3	513.8 ± 24.8	0.569 ± 0.152	0.540 ± 0.072	−0.53 ± 0.8
	20	712.4 ± 157.96	714.7 ± 223.7	0.630 ± 0.116	0.844 ± 0.149	−5.14 ± 2.0
	50	1040.5 ± 285.7	1271.3 ± 148.8	0.411 ± 0.123	0.614 ± 0.189	−6.34 ± 1.5
	100	1580.3 ± 283.3	1605.8 ± 28.6	0.523 ± 0.236	0.788 ± 0.069	−7.71 ± 0.4
DM	10	314.5 ± 69.8	360.4 ± 74.4	0.426 ± 0.120	0.324 ± 0.135	−2.99 ± 0.7
	20	467.9 ± 56.8	342.5 ± 161.1	0.338 ± 0.360	0.314 ± 0.162	−7.05 ± 3.2
	50	747.7 ± 321.4	736.6 ± 218.9	0.643 ± 0.145	0.643 ± 0.145	−2.63 ± 3.3
	100	926.9 ± 338.4	818.9 ± 55.2	0.733 ± 0.062	0.733 ± 0.062	−5.29 ± 1.6
KF	10	256.3 ± 10.3	223.3 ± 12.6	0.345 ± 0.001	0.367 ± 0.021	−8.47 ± 0.2
	20	300.6 ± 15.2	302.9 ± 25.6	0.312 ± 0.022	0.299 ± 0.028	−6.71 ± 1.7
	50	357.9 ± 33.4	298.4 ± 4.9	0.239 ± 0.012	0.247 ± 0.001	−2.31 ± 0.4
	100	359.6 ± 22.3	288.8 ± 11.7	0.233 ± 0.023	0.215 ± 0.010	−7.04 ± 2.0
dH_2O	10	309.7 ± 14.5	n/a[b]	0.36 ± 0.04	n/a[b]	−8.7 ± 6.4
	20	282.5 ± 14.1	n/a[b]	0.32 ± 0.02	n/a[b]	−17.2 ± 8.0
	50	276.9 ± 14.3	n/a[b]	0.27 ± 0.02	n/a[b]	−16.1 ± 3.4
	100	273.8 ± 5.9	n/a[b]	0.24 ± 0.01	n/a[b]	−10.2 ± 3.2

[a] Data are the mean ± SD of three independent measurements. [b] Not tested.

delivered to the cells and side scatter detected by the flow cytometer. The data are presented as the ratio of the histogram means of the treated population to the control population. This signal appears to be the result of both single and agglomerated nanoparticles located inside the cell that increase the refractive index and, thus, the amount of side-scatter light. We and others have shown a direct relationship between the concentration of nanoparticles and the amount of light scatter measured by flow cytometry, and this relationship has also been confirmed by dark-field microscopy.[32,33,35,39,40]

A representative dark-field microscopy image of a BEAS-2B cell after a 24 h exposure to TiO_2 nanoparticles is shown in Figure 3C. At high concentrations of TiO_2 nanoparticles (20−100 μg/mL), the cytoplasm appears to consist primarily of agglomerates. Microscopy has been used previously by our group and others to visualize nanoparticle interaction with cells.[32,39−46] It should be noted that the nanoparticles (colored white) are not located in or over the nucleus.

In BEAS-2B cells treated with TiO_2 nanoparticles in KF, the cell population displayed a concentration-dependent increase in side scatter (Figure 2B), with a ratio normalized to a control of 22.4 at 100 μg/mL (Supplemental Table 4). However, BEAS-2B cells treated with KB and DM showed lower side-scatter values at all concentrations compared to the KF medium, with DM < KB (Figure 3B). The side-scatter ratios normalized to control for KB and DM were 12.2 and 10.6 at 100 μg/mL, respectively (Supplemental Table 1). This indicates less cellular interaction of TiO_2 nanoparticles dispersed in KB and DM occurs compared with TiO_2 nanoparticles dispersed in KF.

Our data indicate that agglomeration size may play a primary role in cellular interaction of TiO_2 nanoparticles, and the medium composition influences both agglomeration size and, consequently, nanoparticle uptake. TiO_2 nanoparticle uptake has been associated with clathrin-coated endocytosis, caveolin-mediated endocytosis, and macropinocytosis.[47] A study by Tedja *et al.*[48] showed that FBS treatment of TiO_2 nanoparticles similar to those used in our study increased cellular uptake compared to the absence of FBS due to a second phase of uptake between 6 and 24 h. Furthermore, they showed that the cellular uptake of FBS-treated TiO_2 nanoparticles occurred by clathrin-mediated endocytosis and that incubation with antivitronectin antibody reduced the cellular uptake of FBS-treated to the level of non-FBS-treated TiO_2 nanoparticles in A549 cells. In our study, we confirm the cellular uptake results shown by Tedja *et al.* in BEAS-2B cells and additionally show that medium mimicking BAL containing BSA and a surfactant can further reduce cellular uptake. This result may mimic a real-world inhalation exposure more than standard *in vitro* studies due to nanoparticle−protein interactions with BAL, particularly lipids.[49]

Cytotoxicity of TiO_2 Nanoparticles. The viability of BEAS-2B cells treated with TiO_2 nanoparticles in all three treatment media was assessed by live/dead staining and microscopy (Supplemental Figure 7A) using a propidium iodide/calcein AM commercial kit (Invitrogen). A 24 h exposure to TiO_2 in all three treatment media produced a <10% decrease in cell viability at the highest concentration (100 μg/mL). This result was confirmed by the trypan dye exclusion assay (Supplemental Figure 8). A 24 h exposure to 100 μM methyl methanesulfonate (MMS), which was used as a positive cytotoxicity control, confirmed the sensitivity of the live/dead assay, with a mean cytotoxicity of 56% compared with untreated cells (data not shown).

Cytotoxicity is a primary biological end point in determining the toxicity of an environmental contaminant. In this study, we found that TiO_2 nanoparticles were not cytotoxic at any concentration up to 100 μg/mL. This result is in agreement with some reports[5,6] and in disagreement with others[9,11] on the cytotoxicity of TiO_2 nanoparticles.[50] The differences in the literature may be due to the specific mechanism by which certain cytotoxicity assays evaluate cell changes, such as membrane permeability (live/dead and trypan blue assays) *versus* mitochondrial function (3-(4,5-dimethylthiazole-2-yl)-2,5-biphenyl tetrazolium bromide or MTT assay). Some nanoparticles have been shown to cause disruption of the mitochondrial respiratory chain.[20] Several studies have shown the ability of nanoparticles to confound cytotoxicity results by interacting with and/or quenching colorimetric assays, fluorometric dyes, or reaction products in assays such as MTT, neutral red, monosodium salt (WST-1), and Coomassie blue.[20,51−56] Similar to previous studies from our group, we analyzed several images in each replicate experiment to ensure that TiO_2 nanoparticles in each treatment medium did not quench the specific dyes used (Supplemental Figure 7B).[40]

Genotoxicity. We quantified DNA damage by the comet assay in BEAS-2B cells treated with TiO_2 nanoparticles, as shown in Figure 4 and Supplemental Table 2. There was a concentration-dependent increase in DNA damage after TiO_2 nanoparticle exposure in all three treatment media that was weakly genotoxic but statistically significant. However, there were no differences in the slopes of the concentration−response curves of the TiO_2-induced DNA damage in the cells in the three media. The 100 μM MMS (1 h exposure) positive control, run concurrently with each experiment and also shown in Figure 4, elicited a highly significant increase in induced DNA damage in all three treatment media.

Other studies have suggested that the DNA damage induced by TiO_2 nanoparticles detected by the comet assay likely occurs *via* oxidative stress due to hydroxyl radical formation. TiO_2 nanoparticles have been shown to produce ROS *in vitro*[57,58] and by our group as measured by immuno-spin-trapping in a cell-free system.[59] Furthermore, studies have used modified

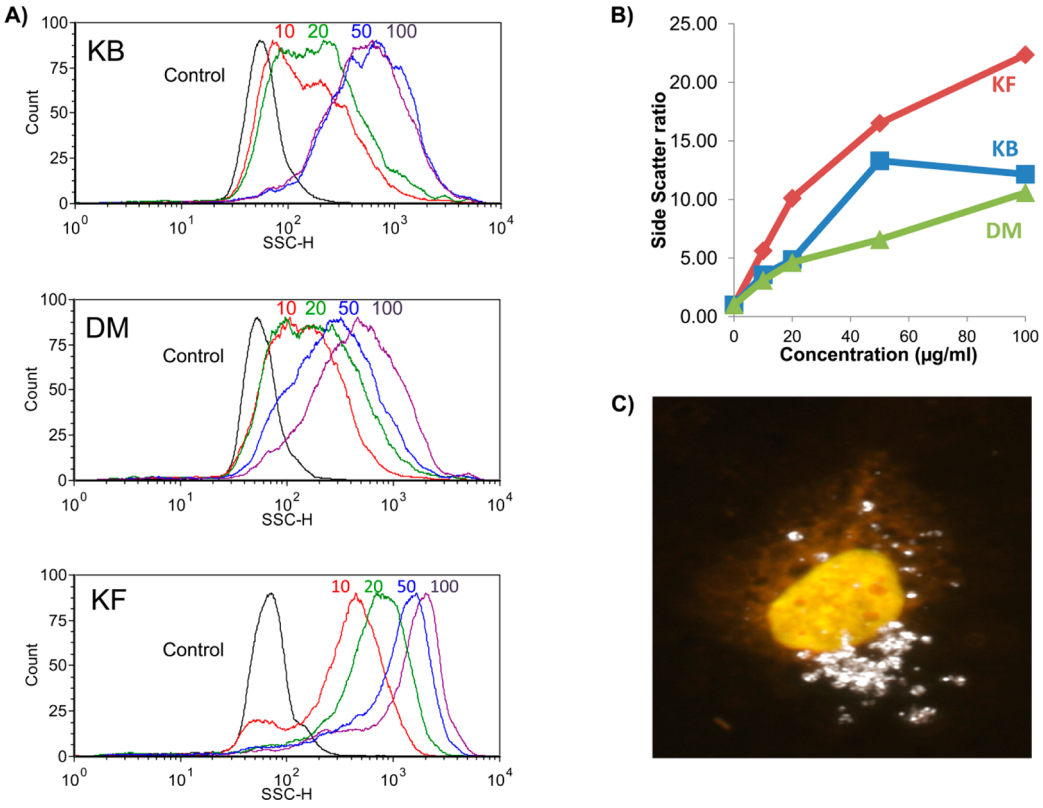

Figure 3. Comparison of cellular interaction of TiO_2 nanoparticles in three different dispersion media (KF, KB, and DM) as revealed by flow cytometer side scatter. (A) Side-scatter histogram profile of cells after exposure to 0, 10, 20, 50, and 100 μg/mL TiO_2 nanoparticles. (B) Representative figure of the mean cell size from the histograms shown in Figure 2A is represented as the ratio of treated to control cells (0 μg/mL). (C) Representative dark-field microscopy image of BEAS-2B cell after a 24 h exposure to TiO_2 nanoparticles stained with 40 μg/mL of acridine orange. A three-color image was acquired using a Nikon E-800 microscope using a FITC filter to observe the nucleus and a TRITC filter to observe the cytoplasm. These fluorescent images were then combined with a dark-field image (white). The Nikon Plan Fluor 60x lens was used with the iris set at ~0.8 NA; magnification was 600×.

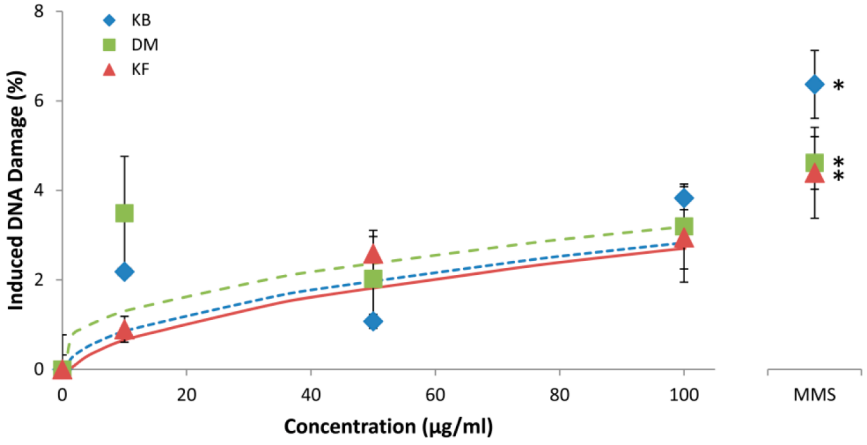

Figure 4. Effect of three different media on the induction of DNA damage (% tail DNA) in the comet assay by TiO_2 nanoparticles in BEAS-2B cells after a 24 h exposure. Data are from three independent experiments normalized by subtracting concurrent negative controls (KB, 2.8 ± 0.3%; DM, 3.7 ± 1.6%; KF, 3.2 ± 0.6%). The positive control (MMS) at 100 μM was used concurrently with each independent experiment (*p < 0.05 from untreated control). Comparison of regression lines showed that there was no effect of medium composition on the induction of DNA damage by the nanoparticles; however, a small but statistically significant increase in DNA damage was shown with increasing concentration (p = 0.0006, R^2 = 0.38). All concentrations in all treatment media induced DNA damage that was significantly greater than the concurrent negative control except for two points: 10 μg/mL in KF and 50 μg/mL in DM.

versions of the comet assay such as formamidopyrimidine DNA-glycosylase treatment to show oxidative stress-induced DNA damage by TiO_2 nanoparticles.[7] Proteomic studies performed by our group on BEAS-2B

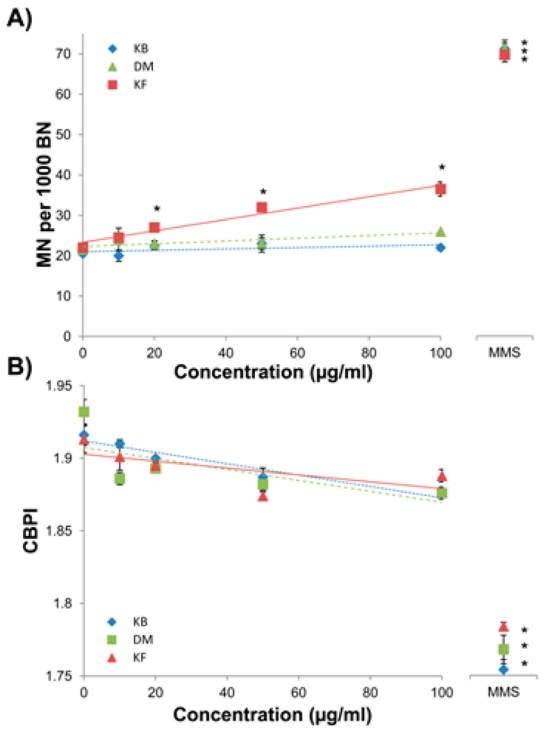

Figure 5. Effect of medium composition on the induction of MN in BEAS-2B cells treated with TiO_2 nanoparticles for 24 h. Data are from two independent experiments. The positive control (100 μM MMS) was used concurrently with each independent experiment and induced significant MN in all treatment media (KB, 71.0 $\pm$ 4.2 MN/1000 BN; DM, 71.0 $\pm$ 2.8 MN/1000 BN; KF, 69.5 $\pm$ 3.5 MN/1000 BN, *$p < 0.05$ from untreated control). (A) Statistical analysis showed that there was no significant induction of MN by TiO_2 nanoparticles in DM or KB media ($p = 0.20$, $R^2 = 0.20$; $p = 0.35$, $R^2 = 0.11$, respectively). However, there was a highly significant induction of MN in cells treated in KF medium ($p < 0.0001$, $R^2 = 0.89$). (B) Cytokinesis-blocked proliferation index (CBPI) showed no difference in treatment medium on cytostasis; however, there was an effect of concentration ($p < 0.05$).

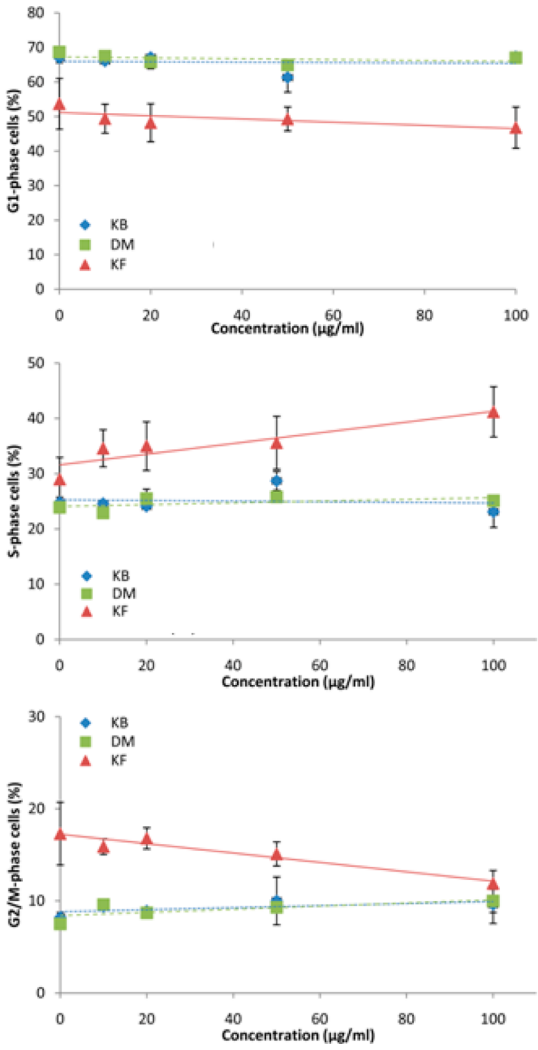

Figure 6. Effect of medium composition on the cell cycle in BEAS-2B cells treated with TiO_2 nanoparticles for 24 h. Data are from two independent experiments. Cell-cycle analysis showed that cells treated with TiO_2 nanoparticles in the KF medium elicited a significant concentration-dependent increase in % of S-phase cells ($p = 0.002$, $R^2 = 0.82$), whereas the cells treated with TiO_2 nanoparticles in the KB and DM media did not.

cells treated with TiO_2 nanoparticles in KB show an increase in expression and activity of two of the most common antioxidant enzymes, catalase and superoxide dismutase. Further, peroxiredoxins and actin proteins known to be associated with the Nrf-2-mediated antioxidative stress pathway were up-regulated as measured by 2D gel electrophoresis analysis.[60] On the basis of our data and the aforementioned studies, we propose that the DNA damage measured by the comet assay may result from ROS.

Chromosome breakage and loss were assessed by the cytokinesis-blocked MN assay, as shown in Figure 5. No increases in MN formation could be shown for BEAS-2B cells treated with any concentration of TiO_2 nanoparticles in KB or DM. However, TiO_2 exposure in KF caused a significant concentration-related increase in MN. The positive control, 100 μM MMS, clearly induced a significant increase in MN in all three treatment media.

The use of serum for *in vitro* nanoparticle studies has been found to influence biological end points and has produced different responses with different types of nanoparticles.[20,30,31,48] When comparing our study to the body of literature on the *in vitro* genotoxicity of TiO_2 nanoparticles, the majority of studies that gave positive results for the MN assay were in cell lines in medium containing 10% or greater FBS in culture and during treatment;[7,10,11] however, those that gave negative results were performed in serum-free medium.[6]

Rahman *et al.*[10] have shown that TiO_2 nanoparticles are clastogenic; thus, the MN seen in our study was due most likely to chromosome breakage. If we assume the MN results are from chromosome breakage and not chromosome loss (aneuploidy), this effect would be dependent on the time of occurrence of the DNA damage in the cell cycle, the type of damage, whether the damage is repaired or not, and the passage of the cells through the cell cycle to the completion of nuclear division.

TABLE 3. Summary of Results

treatment group	media/particle preparation	media/cell treatment	size range at 0 h ($X \pm$ SD)	size range at 24 h ($X \pm$ SD)	cellular interaction ratio (range)	DNA damage (comet)	chromosome damage (MN)	cell-cycle ranges (%)	comments and results
KB	KGM + 0.1% BSA, tip sonicate 2 min	KGM + 0.01% BSA	437.7 ± 115.3 nm to 1580.3 ± 283.3 nm	513.8 ± 24.8 nm to 1605.8 ± 28.6 nm	3.58−12.15	+	−	G1: 61−67 S: 23−29 G2: 8−10	↑ agglomerates ↓ cellular interaction + comet − MN no change: cell cycle
DM	PBS + 0.6% BSA + 0.001% DSPC, cup-horn sonicate 1 h (3 × 20 min, 10 s on/off)	KGM	314.5 ± 69.8 nm to 926.9 ± 338.4 nm	360.4 ± 74.4 nm to 818.9 ± 55.2 nm	3.09−10.58	+	−	G1: 65−69 S: 23−26 G2: 8−10	↑ agglomerates ↓ cellular interaction + comet − MN no change: cell cycle
KF	KGM + 10% FBS, tip sonicate 2 min	KGM + 1% FBS	256.3 ± 10.3 nm to 359.6 ± 22.3 nm	223.3 ± 12.6 nm to 288.8 ± 11.7 nm	5.62 − 22.35	+	+	G1: 47−49 S: 35−41 G2: 12−17	↓ agglomerates ↑ cellular interaction + comet + MN ↑ S-phase cells

Cell Cycle. To determine the effect of TiO_2 nanoparticles in the three treatment media on cell cycle, treated BEAS-2B cells were lysed with nonionic detergent (NP 40), incubated for 15 min at 37 °C, and stained with propidium iodide (PI) as described.[61] The cells were put on ice prior to measuring them in a flow cytometer. As shown in Figure 6, KB- and DM-treated cell populations exposed to different concentrations of TiO_2 nanoparticles had cell-cycle profiles similar to those of untreated control cells. However, TiO_2 nanoparticle-treated BEAS-2B cells in KF showed a significant concentration-dependent increase in the number of S-phase cells (Supplemental Table 3). Other studies on the effects of TiO_2 nanoparticles on cell-cycle progression have found cell-cycle arrest in the short- and long-term.[62,63]

We hypothesize that the effects seen in TiO_2-treated cells in KF are due to nanoparticle−protein interactions that produce small agglomerates, which could be taken into the cell in greater amounts than larger agglomerates. TiO_2 nanoparticles in the cell may induce DNA damage regardless of media composition; however, the agglomerates formed in KF are more likely than agglomerates formed in the other media to induce a type of DNA damage that is processed into MN. In contrast, TiO_2 nanoparticles in KB and DM produced large TiO_2 nanoparticle agglomerates that were not taken up as readily into the cell, and although DNA damage (comet) was induced by such agglomerates, these agglomerates were clearly unable to induce MN.

DM, which contained a surfactant to mimic bronchial-alveolar fluid, served as a model for human inhalation exposure, whereas KF contained serum proteins that may mimic blood. Our results showed that TiO_2 nanoparticles induced a higher frequency of MN in KF than in DM, suggesting that TiO_2 might be more genotoxic *via* ingestion than inhalation. Indeed, such results have been found *in vivo* in mice where 5 days of ingestion of TiO_2 nanoparticles in drinking water induced clastogenicity, genotoxicity, oxidative damage, and inflammation,[64] but 5 days of inhalation exposure induced only inflammation but no genotoxicity.[65] The *in vitro* model used in our study is consistent with *in vivo* findings and clearly shows that there may be health effects associated with nanoscale *versus* micrometer-scale agglomerates of the same type of nanoparticle.[2] This finding is important because there are real-world exposures to a wide range of agglomerated nanoparticles. Future needs are to identify the size of agglomerates that can lead to adverse outcomes. These studies and our data suggest that the route of exposure may play a critical role in the potential genotoxicity of TiO_2 nanoparticles to humans.

A limitation of this study is the various ways in which the nanoparticles were prepared. We note that the preparation procedures involved in the dispersal and sonication of TiO_2 nanoparticles in each treatment medium differ. Also, the addition of serum could potentially act to differentiate the BEAS-2B cells. However, we derive our conclusions from cytotoxicity, cell-cycle populations in the untreated controls and the cytokinesis-blocked proliferation index data (Supplemental Figures 6 and 7, Figure 5B, and Figure 6) that show no significant differences among the treatment media at all concentrations tested. In addition, comparison of the negative and positive controls across all assays showed no effect of treatment media. Additional studies are needed on the ability of nanoparticles to bind to extracellular and intracellular proteins, the mechanism of cellular interaction/uptake, and subsequent mechanisms of toxicity.

CONCLUSIONS

As summarized in Table 3, we have identified the physicochemical characteristics of TiO_2 nanoparticles, their cellular uptake, and their ability to induce genotoxicity and alter the cell cycle in three treatment media of various compositions, defined by protein and lipid concentration. The results showed that the particles agglomerated less in particle-treatment medium that contained 10% FBS (KF) compared to medium with less protein (KB) or medium composed of less protein + surfactant (DM). We find that the smaller TiO_2 nanoparticle agglomerates, which occur in the KF medium, interact more with the cells than do those formed in the other two media, which are larger agglomerates. This result is likely due to the protein corona formed in KF relative to the other two media. The DNA damage as measured by the comet assay was induced equally by the nanoparticles in all three media, indicating that the hydrodynamic diameter of the agglomerates had no influence on the ability of the nanoparticles to induce DNA damage as measured by the comet assay. In contrast, the consequence of the differential agglomeration and particle interaction among the media is that the chromosomal damage as measured by the MN assay and the increased percentage of S-phase cells occurs only in the KF medium, due to the protein in this medium relative to the other two media.

MATERIALS AND METHODS

Chemicals and Instruments. The TiO_2 nanoparticles (86% anatase and 14% rutile as listed by the manufacturer) were obtained from Degussa (now Evonik, AEROXIDE TiO_2 P25, Parsippany, NJ). Particles were sonicated using a probe sonicator (Cole Parmer, Vernon Hills, IL) and a Misonix S-4000 cup-horn sonicator (Cole Parmer). Particle sizing and elemental analysis in the dry form were performed by TEM and ion-coupled plasmon mass spectrometry at the University of Kentucky (Contract #PR-NC-08-10414).[41] TiO_2 dispersions were characterized for hydrodynamic diameter and zeta-potential by dynamic light scattering (DLS)

using a Zetasizer Nano (Malvern Instruments, Worcestershire, UK). The average particle size in the dry form was determined as an arithmetic mean of the measured diameters of approximately 150 particles. Elemental analysis was performed by ICP/MS in duplicate, and specific surface area was determined by BET.[41]

We used three different nanoparticle-treatment media. A medium with a low concentration of protein (KB) was composed of KGM (Lonza, Walkersville, MD) plus 0.1% BSA (Sigma, St. Louis, MO). The dispersion medium (DM) was composed of PBS supplemented with a moderate level of protein in the form of BSA at 6.0 mg/mL (0.6%) and 1,2-dipalmitoyl-*sn*-glycero-3-phosphocholine (DSPC) at 10 μg/mL (0.001%) and was purchased from Sigma-Aldrich. A serum-containing medium (KF) was composed of KGM plus 10% FBS (Invitrogen).

Particle Preparation. For the KB or KF dispersion, preweighed TiO_2 nanoparticles were suspended in KGM medium with 0.1% BSA (KB) or KGM with 10% FBS (KF) at 1 mg/mL and probe sonicated at 7 W for 2 min on ice; subsequent dilutions in KB and KF were made to 500, 200, and 100 μg/mL.

For the DM dispersion, the protocol of Porter *et al.*[49] was used with some modifications. For the preparation of this treatment medium, stock concentrations of 10 mg/mL DSPC were prepared in 100% ethanol, and BSA was made at a concentration of 10 mg/mL. The final concentration of BSA was 0.6% and that of DSPC was 0.001%. The TiO_2 nanoparticles were suspended at a stock concentration of 1 mg/mL and sonicated using a cup-horn sonicator at 78−82 W for 1 h using a 10 s on, 10 s off protocol. Every 20 min, the samples were removed and vortexed to ensure a homogeneous mixture. The particles were then centrifuged at 12 000*g* for 10 min, the supernatant was aspirated, and the protein- and lipid-coated nanoparticles were resuspended in KGM medium. Subsequent dilutions were performed in the same manner as were particles suspended in KB and KF.

Particle Characterization. Nanoparticles were characterized in dry form using TEM (University of Kentucky) and in medium using DLS and zeta-potential measurement techniques. All nanomaterial preparations were diluted 1:10 in KGM and subjected to dynamic light scattering analysis at 0 and 24 h for size and zeta-potential measurements and calculations. Approximately 1 mL of each concentration (0, 10, 20, 50, and 100 μg/mL) was placed in a sizing cuvette (Sarstedt, Nümbrecht, Germany) and measured by the Zetasizer Nano at 37 °C (Malvern Instruments, Worcestershire, UK). Intensity and PdI measurements at each concentration were at 0 and 24 h. The refractive index used for the measurements was 2.51, reflecting a 14% rutile and 86% anatase mixture. Samples were placed in a humidified incubator at 37 °C between measurements. For zeta-potential, each concentration was measured using a zeta-potential cuvette (Malvern Instruments, Worcestershire, UK) at 0 h time point only. All particle characterization measurements are the mean ± SD of three independent experiments.

Scanning Electron Microscopy. Stock TiO_2 nanoparticle suspensions were prepared as described previously in different treatment media at a concentration of 1 mg/mL. Suspensions were then subsequently diluted 1:5 in PTFE-capped glass vials (VWR International, Morrisville, NC) using their original treatment media. Diluted TiO_2 nanoparticle suspensions were mixed, and 5 μL of each sample was placed in the center of a prewarmed (45−50 °C) 0.2 μm nylon membrane filter (P/N 66600, 13 mm diameter, Pall Life Sciences, Ann Arbor, MI) and allowed to dry rapidly. Filters containing the various diluted nanoparticle samples were stored in glass Petri dishes treated for antistatic using Zerostat (Z108812-1EA, Zerostat antistatic instrument, Sigma-Aldrich) at room temperature until analyzed by SEM. SEM micrographs of nylon filters containing various nanoparticle dispersion samples were obtained using the Phenom Tabletop SEM (Phenom-World NA, Inc., Beaverton, OR). Briefly, nylon filters were mounted onto metal stubs using double-backed adhesive carbon tape. The immobilized filter on the stubs was placed in the sample holder and the height adjusted so that the top of the filter was ~2 mm below the holder's surface. The holder was placed in the Phenom and loaded automatically. At the low magnification, our detection limit is 100 nm without carbon coating; with carbon coating, the vendor specifies the lower size limit as 30 nm. Magnification, focus, brightness/contrast, sample position, and image gathering were carried out by the use of an integrated touch screen and rotary adjustment knob according to the manufacturer's instructions.

One-Dimensional Gel Electrophoresis. To determine the proteins adsorbed onto the surface of the TiO_2 nanoparticles in each treatment medium, SDS-PAGE gel electrophoresis of the nanoparticles in each treatment medium, along with the treatment medium alone, was performed as described previously, with some modifications.[12,15,48,66] TiO_2 nanoparticles were diluted in each treatment medium (KB, DM, and KF) at 1 mg/mL and sonicated as described previously. After incubation for 24 h, 1 mL of each suspension was transferred to a separate tube and centrifuged at 12 000*g* for 15 min. The supernatant was aspirated, and the remaining pellets were washed with PBS and centrifuged again. After the supernatant was removed, the TiO_2 nanoparticles and equal volumes of each treatment medium were mixed with 2X Protein Gel Loading Buffer (Fisher Scientific) and heated at 95 °C for 10 min. All samples (treatment medium alone and TiO_2 nanoparticles in each treatment medium) were loaded onto 8−16% SDS-PAGE 1D gels (Thermo Scientific) along with a Fermentas PageRuler Plus protein ladder (Thermo Scientific), and a constant voltage of 125 V for 45 min was applied. The gel was fixed with water for 15 min, stained using Gel Code Blue Stain (Thermo Scientific) for 3 h, followed by destaining with water for ~1 h. Gel images were taken using a Gel Logic 2200 Pro imager and analyzed with MI SE 534 program (Carestream Health, Rochester, NY). Three independent experiments were performed to ensure reproducibility. A representative gel is shown in Supplemental Figure 5.

Cell Treatment. Cells at 5.0×10^4 cells/cm^2 were seeded in T-25 flasks, incubated for 48 h and then treated for 24 h with nanoparticles. For these treatments, the new nanoparticle preparations (KB, DM, and KF) were diluted 1:10 in KGM to provide concentrations of 0, 10, 20 (except for the comet assay), 50, and 100 μg/mL TiO_2. For the MN assay, the cells were treated at ~60% confluence to ensure growth-phase characteristics, and fresh medium was added with the cytochalasin B treatment. For the comet assay, the cells were treated at ~80% confluence.

Cell Line and Cell Culture. BEAS-2B (ATCC), a human bronchial epithelial cell line, was maintained in serum-free keratinocyte basal medium (KBM, Lonza) supplemented with KGM SingleQuots (Lonza) and used at passages 45−60. BEAS-2B cells were infected with a 12-SV40 adenovirus hybrid and cloned (ATCC). Cells were seeded in T-25 tissue culture flasks at a cell density of 5×10^4 cells/cm^2 and incubated in a fully humidified atmosphere at 37 °C with 5% CO_2. The cells were subcultured every 3−4 days or when they reached 85−90% confluency using HBSS (Lonza), Versene (Invitrogen), TrypLE (Invitrogen), and trypsin neutralizing solution (Lonza). Cells were centrifuged at 135*g* for 5 min, the supernatant was aspirated, and the cell pellet was resuspended in fresh medium and brought to a concentration of 5×10^4 cells/cm^2. The cytochalasin B was dissolved in PBS at 1 mg/mL. For the comet assay, SYBR-Gold was purchased from Molecular Probes (Eugene, OR) and diluted 1:200 in 1× TE buffer.

Live/Dead Assay. Calcein-AM and propidium iodide were purchased from Invitrogen (Carlsbad, CA). After cells were incubated in TiO_2 in appropriate medium for 24 h in 25 cm^2 flasks, the medium was aspirated and replaced with fresh medium containing calcein-AM (Invitrogen) and propidium iodide (Invitrogen) at a concentration of 1 μg/mL and placed in a humidified incubator at 37 °C and 5% CO_2 for 1 h. Images were taken of each concentration with WASABI imaging software (Hamamatsu) using an ORCA-ER camera (Hamamatsu) and a phase objective (Nikon, Plan 10×, NA = 0.3), Nikon Diaphot 300 microscope with DAPI and FITC filters. Pictures were evaluated using a scoring grid placed on the captured images. Approximately 200 cells were counted in both live (calcein$^+$) and dead (propidium iodide$^+$) images (Supplemental Figure 6B). Live/dead experiments were performed as three independent 24 h exposures for each treatment medium.

Trypan Blue Dye Exclusion Assay. Trypan blue was purchased from Sigma-Aldrich, and the trypan blue dye exclusion assay was performed to measure the percent viable cells.[67] Briefly,

after treatment, the cells were trypsinized, and 0.1 mL of the whole cell suspension was removed and placed in 0.5 mL of trypan blue and 0.4 mL of sterile PBS at a ratio of 1:10 for each treatment concentration. Counts were performed with a hemocytometer where unstained cells were alive, and those that were stained blue were considered dead. Trypan blue experiments were performed as three independent 24 h exposures for each treatment medium (Supplemental Figure 7).

Flow Cytometry. To determine cellular uptake by flow cytometry, the method of Zucker *et al.*[32,33] was used. Briefly, BEAS-2B cells were plated in 20 T-25 flasks (1×10^5 cells/mL, 5 mL/flask) and incubated for 48 h. After incubation, 10, 20, 50, and 100 μg/mL of TiO_2 nanoparticles was prepared by sonication in three different media (KF, KB, and DM) as described previously. The medium in each flask was replaced with 5 mL of nano-TiO_2 suspension. Each flask received treatment of TiO_2 nanoparticles, and one control flask received only fresh medium. Following 24 h exposure, cells were trypsinized, centrifuged at 135*g* for 10 min, resuspended in 0.5 mL of medium, and put directly on ice. Cellular uptake of TiO_2 nanoparticles was assessed in three independent experiments.

A BD FACSCalibur (BD Biosciences, San Jose, CA) flow cytometer containing a 488 nm laser, forward-scatter (FSC) diode detector, and photomultiplier tube side-scatter (SSC) detector was used in this study. Prior to each experiment, the instrument was checked for functionality and performance using Duke 3.0 μm alignment beads.[40,41] The instrument yielded coefficient of variation values below 2% on all fluorescence channels at low flow rates with Duke 3.0 μm alignment beads. The cytometer was set up to measure SSC logarithmically and FSC linearly. Most of the dynamic ranges of the scales were used to optimize the changes with the different concentrations. The highest concentration of nanoparticles was run first to set the range for the maximum SSC signal and the minimum FSC signal. The treated values were normalized to control values and expressed as percent increase.

Microscopy. Dark-field microscopy has been used by us and others to visualize nanoparticle uptake into cells.[32,33,41−47] The cells in Figure 2C were spun onto a slide using a Shannon CytoSpin centrifuge at 40*g* for 5 min, fixed with 100% methanol, and stained with 40 μg/mL acridine orange for 60 s. A Nikon E-800 microscope was used to observe dark-field and fluorescence images. The fluorescence excitation cubes consisted of FITC and TRITC. However, the dark-field image was so bright that it could be observed through either of the filter cubes. The dark field was ~100 times brighter than the fluorescence image as measured by exposure times. The combination of fluorescence and dark-field images was made sequentially with Nikon Elements software. Colocalization was checked and measured with 0.5 μm Tetra spec beads (Molecular Probes, Eugene, OR), and there was minimal distortion. A xenon light supply was used to optimize the shorter wavelength excitation that provided for better resolution for the dark-field image. A GG420 filter was put in the eyepieces to protect the user's eyes from possible UV damage from the xenon light source.

The most suitable Nikon lens when using a Nikon infinity-corrected microscope was a 60x Plan Fluor with an iris diaphragm to control the numerical aperture (NA) between 0.55 and 1.25. The lens had a sufficiently large magnification to observe cellular details and the background scatter, which could be controlled by adjusting the diaphragm. During the course of this study, the dark-field images were obtained using the following dry lenses, Plan Apo 20x (NA 0.75), and the following oil lenses, 20x multi-immersion (MI, NA 0.75), and 60x Plan Fluor with iris (NA 1.25−0.55).

Comet Assay. The comet assay was performed as described previously.[68] After treatment, the cells were trypsinized and kept on ice throughout the duration of the slide preparation. All nanoparticle concentrations examined resulted in cell viabilities above 80%. Briefly, 10 μL of cells at 10^6 cells/mL (approximately 10 000 cells) was added to 190 μL of 0.53% low-melting-point agarose (LMP), and 90 μL was placed on two slides and covered by a 24 × 50 mm coverslip and placed on ice. After the agarose had solidified, the coverslip was removed, and another 90 μL of LMP was added, and a coverslip was placed on top. The coverslip was removed again, and the slides were placed in 4 °C lysis buffer (5 M NaCl, 100 mM EDTA, 10 mM Tris, 1% Triton X-100, pH 10.0) overnight at 4 °C. Following lysis, slides were rinsed with cold water and immersed in 4 °C denaturing electrophoresis buffer (300 mM NaOH, 1 mM EDTA) for 40 min. Electrophoresis was performed in cold buffer (pH >13) for 20 min at 25 V (1.33 V/cm) and 300 mA. Then the slides were immersed in neutralizing buffer (0.4 M Tris-HCl, pH 7.5) for 15 min, dehydrated in 95% ethanol for 3 min, and allowed to air-dry.

After drying, slides were stained with 5X SYBR-Gold and viewed using fluorescence microscopy. Images were collected using the 25× objective (Plan Fluor 25×, Nikon Microphot FXA), a Nikon B-2H filter, and an ORCA CCD camera (Hamamatsu) connected to a personal computer. Images were analyzed using Komet version 5.5 (Andor Technology, Morrisville, NC); 50 images per slide and two slides per concentration were analyzed in each experiment. Slides were coded before analysis so that the scorer had no knowledge of the treatment when obtaining the data. Data were expressed as the mean ± SD of three independent experiments for each treatment medium and concentration tested. A representative image of undamaged and damaged cells is shown in Supplemental Figure 9.

Cytokinesis-Blocked MN Assay with Acridine Orange Staining. The MN assay with acridine orange staining was performed as described previously.[69] Cells treated with TiO_2 nanoparticles for 24 h and then 5 μg/mL of cytochalasin B for 18 h were resuspended in PBS at a density of 2×10^5 cells/mL. The cells from 75 μL of cell suspension were deposited onto precleaned slides using a Shannon CytoSpin centrifuge at 40*g* for 5 min. Slides were air-dried, fixed in 100% methanol for 10 min, and stored at 20 °C.

Slides were stained in acridine orange diluted to 40 μg/mL in a 0.02 M phosphate buffer (pH 7.4) for 30−45 s and washed twice with distilled water. A 24 × 55 cm cover glass was mounted using Sorenson's buffer (70 mL of 0.1 M $NaHPO_4$ and 30 mL of 0.1 M KH_2PO_4, pH 7.4). Slides were scored blindly using a microscope (Nikon Microphot FXA), dual band-pass filter (TRITC/FITC), and 20× objective (Plan Fluor). We examined 1000 binucleated cells and scored for the presence of MN for each exposure. Scoring criteria followed the recommendations of Fenech *et al.*[70] Additionally, the CBPI was calculated for determination of cytostasis and as a marker of cytotoxicity.[71] Two independent experiments were conducted for all concentrations in all three treatment media.

Cell Cycle. For cell-cycle analysis, BEAS-2B cells were treated with TiO_2 nanoparticles for 24 h in the three different treatment media (KF, KB, and DM), trypsinized, and placed on ice as described above. Cells were then prepared for flow cytometry analysis by incubating them for 15 min at 37 °C with a 1:2 dilution in 0.5% NP-40 nonionic detergent that was made up in PBS without Ca^{2+} and Mg^{2+}. The cells were then stained with propidium iodide (20 μg/mL, Molecular Probes, Eugene OR). The flow cytometer was set to measure nuclei using DNA FL2H (585/42) as the detection trigger. Nuclei subpopulations were analyzed using MultiCycle (Phoenix Flow Systems, San Diego, CA) that was incorporated into FCS express 4.0 (Denovo, Los Angeles, CA) analysis software. The percentages of cells in G1, S, and G2/M phases for all concentrations in each treatment medium were calculated from histograms using the area parameter. Two independent experiments were performed and expressed as mean ± SD (Figure 6), and a representative experiment is shown in Supplemental Table 3.

Statistical Analyses. For statistical analyses, *n* equaled the number of replicate experiments, and results are presented as the mean ± SD. Statistical analyses were carried out by using a one-tailed analysis of variance (ANOVA), where appropriate, followed by Fisher's protected least-significant-difference test for *post-hoc* comparisons to determine if the experimental treatments produced differences among each other or from the controls. Results were considered statistically significant if $p < 0.05$.

In addition, for the comet assay, a linear model was used to compare the slopes of the three regression lines (each treatment medium) for the induced DNA damage *versus* the square root of the concentration after a preliminary analysis for a best-fit model. The induced DNA damage (*i.e.*, % tail DNA of each treated concentration minus mean % tail DNA for the concurrent controls) was used as a measure of damage to normalize the

data because each replicate experiment was done at a different time. The slopes of the regression lines were compared assuming a common *Y*-intercept set to zero using Statgraphics Centurion XVI version 16.1.05 (Statpoint Technologies, Inc., Warranton, VA). For the MN assay, simple linear regression analyses were performed with StatGraphics Centurion XVI for each concentration–response curve for each medium. For the two independent cell-cycle experiments for each medium, linear regression analysis was performed similar to that done by Potter *et al.*[72,73] but only on the change in percentage of cells in S phase. If $p < 0.05$, then the regression was deemed significant, and the medium caused an effect on cell cycle.

Disclosure: This manuscript was reviewed by the National Health and Environmental Effects Research Laboratory, U.S. Environmental Protection Agency and approved for publication. Approval does not signify that the contents necessarily reflect the views and policies of the Agency nor does mention of trade names or commercial products constitute endorsement or recommendation for use.

Conflict of Interest: The authors declare no competing financial interest.

Acknowledgment. The authors would like to thank the University of Kentucky for TEM experiments (PR-NC-08-10414); R. Jaskot for assistance with the SEM studies; J. G. Muñiz Ortiz, J. Campbell, B. Collins, and J. Allen for assistance with the genotoxicity studies; S. Kumar and P. Bommineni for assistance with the study, and K. Tarpley for figure preparation. We also thank the NHEERL Nano Health Effects Team for their help and guidance in this study. The authors would like to thank W. Boyes, B. Collins, and K. Kitchin for in-house review of the manuscript. This study was funded by the U.S. Environmental Protection Agency's intramural research program.

Supporting Information Available: Additional DLS analyses of all concentrations used in genotoxicity studies of TiO_2 nanoparticles suspended in all three treatment media (KB, DM, and KF); sample SEM and TEM images of TiO_2 nanoparticles in dry form and each treatment medium; additional cellular tests using the trypan blue dye exclusion and live/dead assay to determine cytotoxicity; sample images of the comet assay; tables of DLS of TiO_2 nanoparticles diluted in H_2O; PdI and zeta-potential measurements; SSC measurements for all three treatment media for cellular uptake studies; comet assay results; and representative cell-cycle results. This material is available free of charge *via* the Internet at http://pubs.acs.org.

REFERENCES AND NOTES

1. Singh, N.; Manshian, B.; Jenkins, G. J.; Griffiths, S. M.; Williams, P. M.; Maffeis, T. G.; Wright, C. J.; Doak, S. H. Nanogenotoxicology: The DNA Damaging Potential of Engineered Nanomaterials. *Biomaterials* **2009**, *30*, 3891–3914.
2. NIOSH. Current Intelligence Bulletin 63: Occupational Exposure to Titanium Dioxide. *DHHS (NIOSH) Publication* [Online], 2011; pp 2011–2160. http://www.cdc.gov/niosh/docs/2011-160/pdfs/2011-160.pdf.
3. Warheit, D. B.; Webb, T. R.; Reed, K. L.; Frerichs, S.; Sayes, C. M. Pulmonary Toxicity Study in Rats with Three Forms of Ultrafine-TiO_2 Particles: Differential Responses Related to Surface Properties. *Toxicology* **2007**, *230*, 90–104.
4. Hackenberg, S.; Friehs, G.; Kessler, M.; Froelich, K.; Ginzkey, C.; Koehler, C.; Scherzed, A.; Burghartz, M.; Kleinsasser, N. Nanosized Titanium Dioxide Particles Do Not Induce DNA Damage in Human Peripheral Blood Lymphocytes. *Environ. Mol. Mutagen.* **2011**, *52*, 264–268.
5. Bhattacharya, K.; Davoren, M.; Boertz, J.; Schins, R. P.; Hoffmann, E.; Dopp, E. Titanium Dioxide Nanoparticles Induce Oxidative Stress and DNA-Adduct Formation but Not DNA-Breakage in Human Lung Cells. *Part. Fibre Toxicol.* **2009**, *6*, 17.
6. Falck, G. C.; Lindberg, H. K.; Suhonen, S.; Vippola, M.; Vanhala, E.; Catalan, J.; Savolainen, K.; Norppa, H. Genotoxic Effects of Nanosized and Fine TiO_2. *Hum. Exp. Toxicol.* **2009**, *28*, 339–352.
7. Gurr, J. R.; Wang, A. S.; Chen, C. H.; Jan, K. Y. Ultrafine Titanium Dioxide Particles in the Absence of Photoactivation Can Induce Oxidative Damage to Human Bronchial Epithelial Cells. *Toxicology* **2005**, *213*, 66–73.
8. Hackenberg, S.; Friehs, G.; Froelich, K.; Ginzkey, C.; Koehler, C.; Scherzed, A.; Burghartz, M.; Hagen, R.; Kleinsasser, N. Intracellular Distribution, Geno- and Cytotoxic Effects of Nanosized Titanium Dioxide Particles in the Anatase Crystal Phase on Human Nasal Mucosa Cells. *Toxicol. Lett.* **2010**, *195*, 9–14.
9. Kang, S. J.; Kim, B. M.; Lee, Y. J.; Chung, H. W. Titanium Dioxide Nanoparticles Trigger P53-Mediated Damage Response in Peripheral Blood Lymphocytes. *Environ. Mol. Mutagen.* **2008**, *49*, 399–405.
10. Rahman, Q.; Lohani, M.; Dopp, E.; Pemsel, H.; Jonas, L.; Weiss, D. G.; Schiffmann, D. Evidence That Ultrafine Titanium Dioxide Induces Micronuclei and Apoptosis in Syrian Hamster Embryo Fibroblasts. *Environ. Health Perspect.* **2002**, *110*, 797–800.
11. Wang, J. J.; Sanderson, B. J.; Wang, H. Cyto- and Genotoxicity of Ultrafine TiO_2 Particles in Cultured Human Lymphoblastoid Cells. *Mutat. Res.* **2007**, *628*, 99–106.
12. Maiorano, G.; Sabella, S.; Sorce, B.; Brunetti, V.; Malvindi, M. A.; Cingolani, R.; Pompa, P. P. Effects of Cell Culture Media on the Dynamic Formation of Protein–Nanoparticle Complexes and Influence on the Cellular Response. *ACS Nano* **2010**, *4*, 7481–7491.
13. Dutta, D.; Sundaram, S. K.; Teeguarden, J. G.; Riley, B. J.; Fifield, L. S.; Jacobs, J. M.; Addleman, S. R.; Kaysen, G. A.; Moudgil, B. M.; Weber, T. J. Adsorbed Proteins Influence the Biological Activity and Molecular Targeting of Nanomaterials. *Toxicol. Sci.* **2007**, *100*, 303–315.
14. Monopoli, M. P.; Walczyk, D.; Campbell, A.; Elia, G.; Lynch, I.; Bombelli, F. B.; Dawson, K. A. Physical–Chemical Aspects of Protein Corona: Relevance to *In Vitro* and *In Vivo* Biological Impacts of Nanoparticles. *J. Am. Chem. Soc.* **2011**, *133*, 2525–2534.
15. Lundqvist, M.; Stigler, J.; Elia, G.; Lynch, I.; Cedervall, T.; Dawson, K. A. Nanoparticle Size and Surface Properties Determine the Protein Corona with Possible Implications for Biological Impacts. *Proc. Natl. Acad. Sci. U.S.A.* **2008**, *105*, 14265–14270.
16. Nel, A. E.; Madler, L.; Velegol, D.; Xia, T.; Hoek, E. M.; Somasundaran, P.; Klaessig, F.; Castranova, V.; Thompson, M. Understanding Biophysicochemical Interactions at the Nano-Bio Interface. *Nat. Mater.* **2009**, *8*, 543–557.
17. Foucaud, L.; Wilson, M. R.; Brown, D. M.; Stone, V. Measurement of Reactive Species Production by Nanoparticles Prepared in Biologically Relevant Media. *Toxicol. Lett.* **2007**, *174*, 1–9.
18. Hauck, T. S.; Ghazani, A. A.; Chan, W. C. Assessing the Effect of Surface Chemistry on Gold Nanorod Uptake, Toxicity, and Gene Expression in Mammalian Cells. *Small* **2008**, *4*, 153–159.
19. Sager, T. M. P.; D, W.; Robinson, V. A.; Lindsley, W. G.; Schwegler-Berry, D. E.; Castranova, V. Improved Method To Disperse Nanoparticles for *In Vitro* and *In Vivo* Investigation of Toxicity. *Nanotoxicology* **2007**, *1*, 118–129.
20. Doak, S. H.; Griffiths, S. M.; Manshian, B.; Singh, N.; Williams, P. M.; Brown, A. P.; Jenkins, G. J. Confounding Experimental Considerations in Nanogenotoxicology. *Mutagenesis* **2009**, *24*, 285–293.
21. Johnston, H. J.; Hutchison, G. R.; Christensen, F. M.; Peters, S.; Hankin, S.; Stone, V. Identification of the Mechanisms That Drive the Toxicity of TiO_2 Particulates: The Contribution of Physicochemical Characteristics. *Part. Fibre Toxicol.* **2009**, *6*, 33.
22. Donaldson, K.; Poland, C. A.; Schins, R. P. Possible Genotoxic Mechanisms of Nanoparticles: Criteria for Improved Test Strategies. *Nanotoxicology* **2010**, *4*, 414–420.
23. Gonzalez, L.; Lison, D.; Kirsch-Volders, M. Genotoxicity of Engineered Nanomaterials: A Critical Review. *Nanotoxicology* **2008**, *2*, 252–273.
24. Wick, P.; Manser, P.; Limbach, L. K.; Dettlaff-Weglikowska, U.; Krumeich, F.; Roth, S.; Stark, W. J.; Bruinink, A. The Degree and Kind of Agglomeration Affect Carbon Nanotube Cytotoxicity. *Toxicol. Lett.* **2007**, *168*, 121–131.

25. Stone, V.; Johnston, H.; Schins, R. P. Development of *In Vitro* Systems for Nanotoxicology: Methodological Considerations. *Crit. Rev. Toxicol.* **2009**, *39*, 613–626.
26. Ji, Z.; Jin, X.; George, S.; Xia, T.; Meng, H.; Wang, X.; Suarez, E.; Zhang, H.; Hoek, E. M.; Godwin, H.; *et al.* Dispersion and Stability Optimization of TiO_2 Nanoparticles in Cell Culture Media. *Environ. Sci. Technol.* **2010**, *44*, 7309–7314.
27. Tenzer, S.; Docter, D.; Rosfa, S.; Wlodarski, A.; Kuharev, J.; Rekik, A.; Knauer, S. K.; Bantz, C.; Nawroth, T.; Bier, C.; *et al.* Nanoparticle Size Is a Critical Physicochemical Determinant of the Human Blood Plasma Corona: A Comprehensive Quantitative Proteomic Analysis. *ACS Nano* **2011**, *5*, 7155–7167.
28. Merhi, M.; Dombu, C. Y.; Brient, A.; Chang, J.; Platel, A.; Le Curieux, F.; Marzin, D.; Nesslany, F.; Betbeder, D. Study of Serum Interaction with a Cationic Nanoparticle: Implications for *In Vitro* Endocytosis, Cytotoxicity and Genotoxicity. *Int. J. Pharm.* **2012**, *423*, 37–44.
29. Corradi, S.; Gonzalez, L.; Thomassen, L. C.; Bilanicova, D.; Birkedal, R. K.; Pojana, G.; Marcomini, A.; Jensen, K. A.; Leyns, L.; Kirsch-Volders, M. Influence of Serum on *In Situ* Proliferation and Genotoxicity in A549 Human Lung Cells Exposed to Nanomaterials. *Mutat. Res.* **2012**, *745*, 21–27.
30. Nel, A.; Xia, T.; Madler, L.; Li, N. Toxic Potential of Materials at the Nanolevel. *Science* **2006**, *311*, 622–627.
31. Maynard, A. D.; Aitken, R. J.; Butz, T.; Colvin, V.; Donaldson, K.; Oberdorster, G.; Philbert, M. A.; Ryan, J.; Seaton, A.; Stone, V.; *et al.* Safe Handling of Nanotechnology. *Nature* **2006**, *444*, 267–269.
32. Zucker, R. M.; Massaro, E. J.; Sanders, K. M.; Degn, L. L.; Boyes, W. K. Detection of TiO_2 Nanoparticles in Cells by Flow Cytometry. *Cytometry, Part A* **2010**, *77*, 677–685.
33. Zucker, R. M.; Daniel, K. M. Detection of TiO_2 Nanoparticles in Cells by Flow Cytometry. *Methods Mol. Biol.* **2012**, *906*, 497–509.
34. Sayes, C. M.; Warheit, D. B. Characterization of Nanomaterials for Toxicity Assessment. *Wiley Interdiscip. Rev. Nanomed. Nanobiotechnol.* **2009**, *1*, 660–670.
35. Renliang, X.; Chifei, W.; Haiyan, X. Particle Size and Zeta Potential of Carbon Black in Liquid Media. *Carbon* **2007**, *45*, 2806–2809.
36. Deng, Z. J.; Mortimer, G.; Schiller, T.; Musumeci, A.; Martin, D.; Minchin, R. F. Differential Plasma Protein Binding to Metal Oxide Nanoparticles. *Nanotechnology* **2009**, *20*, 455101.
37. Horie, M.; Nishio, K.; Fujita, K.; Endoh, S.; Miyauchi, A.; Saito, Y.; Iwahashi, H.; Yamamoto, K.; Murayama, H.; Nakano, H.; *et al.* Protein Adsorption of Ultrafine Metal Oxide and Its Influence on Cytotoxicity toward Cultured Cells. *Chem. Res. Toxicol.* **2009**, *22*, 543–553.
38. Suzuki, H.; Toyooka, T.; Ibuki, Y. Simple and Easy Method To Evaluate Uptake Potential of Nanoparticles in Mammalian Cells Using a Flow Cytometric Light Scatter Analysis. *Environ. Sci. Technol.* **2007**, *41*, 3018–3024.
39. Shapiro, H. M. Optical Measurements in Cytometry: Light Scattering, Extinction, Absorption, and Fluorescence. *Methods Cell. Biol.* **2001**, *63*, 107–129.
40. Zucker, R. M. Flow Cytometry Quality Assurance in Vol. Standardization. In *Fluorometry: State-of-the-Art and Future Challenges*. Wolfbeis, O. S., Ed.; Springer-Verlag: Berlin, 2008; pp 343−370.
41. Sanders, K.; Degn, L. L.; Mundy, W. R.; Zucker, R. M.; Dreher, K.; Zhao, B.; Roberts, J. E.; Boyes, W. K. *In Vitro* Phototoxicity and Hazard Identification of Nano-Scale Titanium Dioxide. *Toxicol. Appl. Pharmacol.* **2012**, *258*, 226–236.
42. Zucker, R. M.; Daniel, K. M. Microscopy Imaging Methods for the Detection of Silver and Titanium Nanoparticles within Cells. *Methods Mol. Biol.* **2012**, *906*, 483–496.
43. Hu, M.; Novo, C.; Funston, A.; Wang, H.; Staleva, H.; Zou, S.; Mulvaney, P.; Xia, Y.; Hartland, G. V. Dark-Field Microscopy Studies of Single Metal Nanoparticles: Understanding the Factors That Influence the Linewidth of the Localized Surface Plasmon Resonance. *J. Mater. Chem.* **2008**, *18*, 1949–1960.
44. Cao, W.; Huang, T.; Xu, X. H.; Elsayed-Ali, H. E. Localized Surface Plasmon Resonance of Single Silver Nanoparticles Studied by Dark-Field Optical Microscopy and Spectroscopy. *J. Appl. Phys.* **2011**, *109*, 34310.
45. Weinkauf, H.; Brehm-Stecher, B. F. Enhanced Dark Field Microscopy for Rapid Artifact-Free Detection of Nanoparticle Binding to *Candida albicans* Cells and Hyphae. *Biotechnol. J.* **2009**, *4*, 871–879.
46. Johnston, H. J.; Semmler-Behnke, M.; Brown, D. M.; Kreyling, W.; Tran, L.; Stone, V. Evaluating the Uptake and Intracellular Fate of Polystyrene Nanoparticles by Primary and Hepatocyte Cell Lines *in Vitro*. *Toxicol. Appl. Pharmacol.* **2010**, *242*, 66–78.
47. Thurn, K. T.; Arora, H.; Paunesku, T.; Wu, A.; Brown, E. M.; Doty, C.; Kremer, J.; Woloschak, G. Endocytosis of Titanium Dioxide Nanoparticles in Prostate Cancer PC-3M Cells. *Nanomedicine* **2011**, *7*, 123–130.
48. Tedja, R.; Lim, M.; Amal, R.; Marquis, C. Effects of Serum Adsorption on Cellular Uptake Profile and Consequent Impact of Titanium Dioxide Nanoparticles on Human Lung Cell Lines. *ACS Nano* **2012**, *6*, 4083–4093.
49. Porter, D.; Sriram, K.; Wolfarth, M.; Jefferson, A.; Schwegler-Berry, D.; Andrew, M.; Castranova, V. A Biocompatible Medium for Nanoparticle Dispersion. *Nanotoxicology* **2008**, *2*, 144–154.
50. Iavicoli, I.; Leso, V.; Fontana, L.; Bergamaschi, A. Toxicological Effects of Titanium Dioxide Nanoparticles: A Review of *In Vitro* Mammalian Studies. *Eur. Rev. Med. Pharmacol. Sci.* **2011**, *15*, 481–508.
51. Belyanskaya, L.; Manser, P.; Spohn, P.; Bruinink, A.; Wick, P. The Reliability and Limits of the MTT Reduction Assay for Carbon Nanotubes−Cell Interaction. *Carbon* **2007**, *45*, 2643–2648.
52. Casey, A.; Herzog, E.; Davoren, M.; Lyn, F. M.; Byrne, H. J.; Chambers, G. Spectroscopic Analysis Confirms the Interactions between Single Walled Carbon Nanotubes and Various Dyes Commonly Used To Assess Cytotoxicity. *Carbon* **2007**, *45*, 1425–1432.
53. Davoren, M. E.; Herzog, E.; Casey, A.; Cottineau, B.; Chambers, G.; Byrne, H. J.; Lyng, F. M. *In Vitro* Toxicity Evaluation of Single Walled Carbon Nanotubes on Human A549 Lung Cells. *Toxicol. in Vitro* **2007**, *21*, 438–448.
54. Hurt, R. H.; Monthioux, M.; Kane, A. Toxicology of Carbon Nanomaterials: Status, Trends, and Perspectives on the Special Issue. *Carbon* **2006**, *44*, 1028–1033.
55. Monteiro-Riviere, N. A.; Inman, A. O. Challenges for Assessing Carbon Nanomaterial Toxicity to the Skin. *Carbon* **2006**, *44*, 1070–1078.
56. Worle-Knirsch, J. M.; Pulskamp, K.; Krug, H. F. Oops They Did it Again! Carbon Nanotubes Hoax Scientists in Viability Assays. *Nano Lett.* **2006**, *6*, 1261–1268.
57. Jaeger, A.; Weiss, D. G.; Jonas, L.; Kriehuber, R. Oxidative Stress-Induced Cytotoxic and Genotoxic Effects of Nano-Sized Titanium Dioxide Particles in Human HaCaT Keratinocytes. *Toxicology* **2012**, *296*, 27–36.
58. Reeves, J. F.; Davies, S. J.; Dodd, N. J.; Jha, A. N. Hydroxyl Radicals (*OH) Are Associated with Titanium Dioxide (TiO_2) Nanoparticle-Induced Cytotoxicity and Oxidative DNA Damage in Fish Cells. *Mutat. Res.* **2008**, *640*, 113–122.
59. Kitchin, K. T.; Prasad, R. Y.; Wallace, K. Oxidative Stress Studies of Six TiO_2 and Two CeO_2 Nanomaterials: Immuno-Spin Trapping Results with DNA. *Nanotoxicology* **2011**, *5*, 546–556.
60. Ge, Y.; Bruno, M.; Wallace, K.; Winnik, W.; Prasad, R. Y. Proteome Profiling Reveals Potential Toxicity and Detoxification Pathways Following Exposure of BEAS-2B Cells to Engineered Nanoparticle Titanium Dioxide. *Proteomics* **2011**, *11*, 2406–2422.
61. Zucker, R. M.; Massaro, E. J.; Elstein, K. H. The Reversibility of Tributyltin-Induced Toxicity *in Vitro* as a Function of Concentration and Duration of Exposure (C X T). *Environ. Res.* **1992**, *57*, 107–116.
62. Wu, J.; Sun, J.; Xue, Y. Involvement of Jnk and P53 Activation in G2/M Cell Cycle Arrest and Apoptosis Induced by Titanium Dioxide Nanoparticles in Neuron Cells. *Toxicol. Lett.* **2010**, *199*, 269–276.
63. Huang, S.; Chueh, P. J.; Lin, Y. W.; Shih, T. S.; Chuang, S. M. Disturbed Mitotic Progression and Genome Segregation Are Involved in Cell Transformation Mediated by Nano-TiO_2 Long-Term Exposure. *Toxicol. Appl. Pharmacol.* **2009**, *241*, 182–194.

64. Trouiller, B.; Reliene, R.; Westbrook, A.; Solaimani, P.; Schiestl, R. H. Titanium Dioxide Nanoparticles Induce DNA Damage and Genetic Instability *in Vivo* in Mice. *Cancer Res.* **2009**, *69*, 8784–8789.
65. Lindberg, H. K.; Falck, G. C.; Catalan, J.; Koivisto, A. J.; Suhonen, S.; Jarventaus, H.; Rossi, E. M.; Nykasenoja, H.; Peltonen, Y.; Moreno, C.; *et al.* Genotoxicity of Inhaled Nanosized TiO_2 in Mice. *Mutat. Res.* **2012**, *745*, 58–64.
66. Tedja, R.; Soeriyadi, A. H.; Whittaker, M. R.; Lim, M.; Marquis, C.; Boyer, C.; Davis, T. P.; Amal, R. Effect of TiO_2 Nanoparticle Surface Functionalization on Protein Adsorption, Cellular Uptake and Cytotoxicity: The Attachment of PEG Comb Polymers Using Catalytic Chain Transfer and Thiol-Ene Chemistry. *Polym. Chem.* **2012**, *3*, 2743–2751.
67. Phillips, H. J. Dye Exclusion Test for Cell Viability. In *Tissue Culture*; Kruse, P. F., Ed.; Academic Press: New York, 1973; pp 407−408.
68. Singh, N. P.; Tice, R. R.; Stephens, R. E.; Schneider, E. L.; Microgel, A. Electrophoresis Technique for the Direct Quantitation of DNA Damage and Repair in Individual Fibroblasts Cultured on Microscope Slides. *Mutat. Res.* **1991**, *252*, 289–296.
69. Ellard, S.; Parry, E. M. A Modified Protocol for the Cytochalasin B *In Vitro* Micronucleus Assay Using Whole Human Blood or Separated Lymphocyte Cultures. *Mutagenesis* **1993**, *8*, 317–320.
70. Fenech, M. The *In Vitro* Micronucleus Technique. *Mutat. Res.* **2000**, *455*, 81–95.
71. Kirsch-Volders, M.; Sofuni, T.; Aardema, M.; Albertini, S.; Eastmond, D.; Fenech, M.; Ishidate, M., Jr.; Kirchner, S.; Lorge, E.; Morita, T.; *et al.* Report from the *In Vitro* Micronucleus Assay Working Group. *Mutat. Res.* **2003**, *540*, 153–163.
72. Potter, A. J.; Gollahon, K. A.; Palanca, B. J.; Harbert, M. J.; Choi, Y. M.; Moskovitz, A. H.; Potter, J. D.; Rabinovitch, P. S. Flow Cytometric Analysis of the Cell Cycle Phase Specificity of DNA Damage Induced by Radiation, Hydrogen Peroxide and Doxorubicin. *Carcinogenesis* **2002**, *23*, 389–401.
73. Potter, A. J.; Rabinovitch, P. S. The Cell Cycle Phases of DNA Damage and Repair Initiated by Topoisomerase II-Targeting Chemotherapeutic Drugs. *Mutat. Res.* **2005**, *572*, 27–44.